

## Special Article

# Analysis of pressure distribution in the foot using finite elements

Carlos Aberto Costa<sup>1</sup> , Vinicius Victorazzi Lain<sup>1</sup> , Alexandre Leme Godoy-Santos<sup>2</sup> , Victor Gonçalves de Antoni<sup>1</sup> , Paulo Roberto Linzmaier<sup>1</sup> , Felipe Acordi Costa<sup>1</sup> 

1. Universidade de Caxias do Sul, Caxias do Sul, RS, Brazil.

2. Lab. Prof Manlio Mario Marco Napoli, Hospital das Clinicas HCFMUSP, Faculdade de Medicina, Universidade de Sao Paulo, Sao Paulo, SP, Brazil.

## Abstract

The objective of this study is to evaluate the applicability of the finite element method to analyze pressure distribution in the healthy human foot. Images of a foot were captured using computed tomography and converted into a three-dimensional model, which was adjusted with the aid of CAD software. The model was imported into Abaqus software for finite element analysis, considering the different regions of the foot. Observations of displacement, stresses, and pressure distribution demonstrated a biomechanical behavior of the foot consistent with that reported in the existing literature, regarding the regions of peak plantar pressure. These findings demonstrate the feasibility of evaluating the physical and mechanical behavior of the human foot using the finite element method, and can serve as a reference for the study and manufacture of orthotic appliances, prosthetic devices, and insoles.

**Level of Evidence V; Prognostic Studies; Expert Opinion.**

**Keywords:** Biomechanics; Foot; Finite element; Diabetic foot; Plantar pressure.

## Introduction

Diabetic neuropathy (DN) is a complication that affects about 50% of patients with diabetes mellitus. It manifests chiefly as loss of sensation<sup>(1)</sup>. In the presence of DN, bone microfractures occur, disrupting the plantar arch, changing the points of support and facilitating loss of skin continuity. Secondary infections are compounded by an associated microangiopathic ischemic state<sup>(2)</sup>. It is estimated that, by the year 2025, approximately 333 million people will have been diagnosed with diabetes worldwide<sup>(3,4)</sup>. This socioeconomic impact highlights the need to assess risk factors for the development of lower-limb ulcers and amputations in patients with diabetes and consequently, the study of pressure overload on the diabetic foot<sup>(5)</sup>.

Pressure distribution in the diabetic foot is usually measured through pressure sensors applied to the patient. However, such devices are limited to foot pressure distribution and do not reveal the internal influences between bones and soft tissue. An alternative approach is the finite element method (FEM), which would allow one to model and simulate the human foot by predicting the distribution of plantar pressure during

use of different shoes, insoles, and orthotic appliances, thus facilitating the manufacture of custom devices for each specific patient. Furthermore, the FEM can also predict the internal forces and deformations of the bones and soft tissues of the foot<sup>(6)</sup>. The present study builds on the work of two groups: Antunes et al. (2007)<sup>(7)</sup> and Cheung and Zhang (2006)<sup>(8)</sup>.

## Methods

Computed tomography scans (slice thickness 0.5mm) of the right ankle and foot of a healthy female volunteer (age 26 years, weight 56kg) with anatomically normal feet were obtained. The captured images were reconstructed as 3D surfaces (STL format) using InVesalius<sup>®</sup> v.3.1 software. Separation masks were used to isolate the anatomical structures of the foot into 31 bones and 1 soft-tissue volume (representing the entire foot). Magics<sup>®</sup> software was used for geometric fine-tuning and smoothing of the STL triangle mesh. The adjusted STL model was then transformed into STEP format<sup>(9)</sup>. Three-dimensional modeling and geometric treatment were performed in the Solidworks<sup>®</sup> software environment. Briefly, a model was created from the bone structure filled with cartilage (Figure 1A).

Study performed at the Universidade de Caxias do Sul, Caxias do Sul, RS, Brazil.

**Correspondence:** Carlos Aberto Costa. 1130 Francisco Getúlio Vargas St., Petrópolis, Caxias do Sul, RS, Brazil, Zip Code: 95070-560. **E-mail:** cacosta@ucs.br.  
**Conflicts of interest:** none. **Source of funding:** own. **Date received:** July 23, 2020. **Date accepted:** July 24, 2020. **Online:** August 30, 2020.

**How to cite this article:** Costa CA, Lain VV, Godoy-Santos AL, Antoni VC, Linzmaier PR, Costa FA. Special article: Analysis of pressure distribution in the foot using finite elements. *J Foot Ankle.* 2020;14(2):197-200.



This bone-and-cartilage model was then subtracted from the overall foot model to obtain a hollow soft-tissue model, i.e., consisting of skin, fat, and muscle alone. These made up the whole study model (Figure 1B, 1C and 1D).

A finite element model (FEM) was created in Abaqus® 6.14-5 software for further simulation, based on the distribution of contact pressures between the ground and the foot. *Tie* and *surface-to-surface* constraints were created for each bone-cartilage pair in the FEM model. This type of constraint links the nodes of the *master* surface to the *slave* surface, transmitting forces from part to part. In this case, the surfaces of the bone-cartilage set were defined as the *master* and the internal surfaces of the soft tissue as *the slave*. The foot-to-ground interface was defined through a pair of *surface-to-surface* interactions which allowed sliding, with the upper surface of the ground as the *master* and the lower sole of the foot as the *slave*. This allows the generation of a contact pressure field on the plantar surface area. A coefficient of friction of 0.6 was defined for the tangential behavior of the contact, while an *Augmented Lagrange* constraint method was used for the normal behavior of the contact.

The materials used in the model were considered isotropic, homogeneous, and linear-elastic, except for the soft tissue, which was set as hyperelastic due to its characteristic nonlinear elastic behavior. The ground was set as a non-deformable rigid material. The plantar fascia was divided into five axes, represented by truss elements with a cross-sectional area of 58.6mm<sup>2</sup>. To account for the key function of the plantar fascia (stabilizing the longitudinal arch of the foot and sustaining high stress levels during weight bearing), the behavior of the truss element was defined as non-compressible. The nominal properties of the materials were obtained from the literature (Table 1). The nonlinear mechanical behavior of the soft tissue was defined by a hyperelastic model, based on a second-order polynomial strain energy function. The parameters were obtained from Antunes et al. (2007)<sup>(7)</sup>.

To generate the mesh, 3D-tetrahedral elements were defined. Linear formulations were used, except for the soft tissue, which used a hybrid formulation instead to ensure the near-incompressible constraint of the nonlinear elastic behavior of the material. All structures, element types, and formulations were based on the work of Antunes et al. (2007)<sup>(7)</sup> and Cheung and Zhang (2006)<sup>(8)</sup> (Table 2). The size of the mesh element was refined on the plantar surface, on the cartilage surfaces in contact with the bone surface, and on the inner soft tissue surface in contact with the bone-cartilage joint. The complete model consists of 680,689 mesh elements.

The load on the posterior face of the calcaneus bone was simulated using five vectors with vertical forces of positive magnitude in the Y-direction<sup>(10)</sup>. As the volunteer in the present case had a body mass of 54 kg, the weight on each foot was 270 N and the force applied on the tendon was 135 N. Thus, a load of 27 N was uniformly applied to each vector and the weight on each foot (270 N) was applied vertically below the support in the positive Y-direction.

The 270-N force represents the reaction of the person's weight, and could only be applied after rendering the upper surfaces of the soft tissue, tibia, and fibula fixed. In addition, a kinematic constraint was defined so as to allow the ground to move only in the positive vertical direction (Y axis), without any possibility of rotational motion.

## Results and Discussion

Displacement was measured by calculating the difference in positions of the nodes before and after application of forces in the model. Figures 2A and 2B show the displacements identified along the Y axis. The peak displacements were

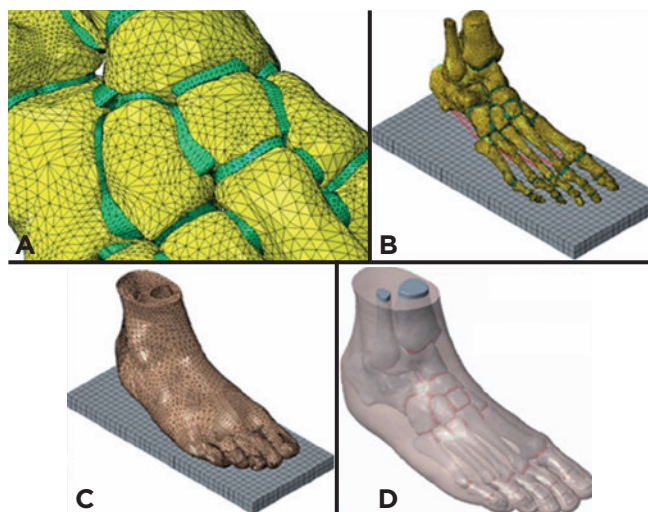


**Figure 1.** A. Modeling and attachment of cartilage elements for bone support; B. Full 3D model; C. Finite-element mesh model.

**Table 1.** Mechanical properties attributed to the study elements

Element	Modulus of elasticity [MPa]	Poisson's ratio (ν)	Cross-section [mm <sup>2</sup> ]
Bone	7,300	0.3	-
Cartilage	10	0.4	-
Soft tissue	Hyperelastic	-	-
Plantar fascia	350	0.4	58.6
Ground	210,000	0.3	-

\*MPa: megapascal / \*\*v - / \*\*\*mm<sup>2</sup>: square millimeter

**Table 2.** Element, type of element, and formulation

Element	Type of element	Formulation
Bone	3D-tetrahedron	Linear
Cartilage	3D-tetrahedron	Linear
Soft tissue	3D-tetrahedron	Linear, hybrid
Plantar fascia	1D-truss	Linear
Floor (Ground)	3D-hexahedron	Linear

-0.875mm in the dark blue region and +4 to +5mm in the area of the metatarsals and phalanges. This is a result of the weight reaction force applied to the foot support (positive Y-direction) exceeding the Achilles tendon force (applied to the upper surface of the calcaneus, positive Y-direction) and the forces applied to the model being displaced away from the fixed surfaces (tibia, fibula, and soft tissue). Thus, the weight reaction force deforms the less rigid regions (soft tissue) and displaces the more rigid structures (bones) upwards. As the bony structure of the foot is rigid and the cross-sectional surfaces are fixed, the foot then pivots, causing downward displacement of the bones of the hindfoot (calcaneus, talus). This is also demonstrated by the decrease in displacement from the region of the phalanges to the region of the fibula and tibia, exhibiting a “relief displacement” pattern.

Figures 2C and 2D show that the interactions and constraints between bone and cartilage have been correctly established. In the bone structure as a whole, peak stress levels of 2 to 4MPa (200 to 400N/cm<sup>2</sup>) are seen in the metatarsals, talus, calcaneus, tibia, and fibula. High peak stresses, e.g., 15.21 MPa (1521N/cm<sup>2</sup>), are also seen at the attachments of the plantar fascia; this is related to tensioning of the truss element.

Regarding plantar pressure distribution, that of the proposed model was consistent with the findings of Hamill et al. (2016)<sup>(11)</sup>. The greatest pressure is seen the heel, followed by the tuberosity of the fifth metatarsal; pressure is then distributed across the heads of the metatarsals, being highest at the first metatarsal, followed by the second and third metatarsals. Furthermore, the “footprint” (i.e., the pressure distribution of the simulated foot) was similar to a flat map obtained by scanning a rigid PU foam cast of the volunteer’s foot (Figures 3A and 3B).

Considering the findings of Cheung and Zhang (2006)<sup>(8)</sup> and Antunes et al. (2007)<sup>(7)</sup>, our results are similar with res-

pect to the distribution of higher and lower pressures, with the exception of the pressure identified on the head of the fourth metatarsal, which was lower in the proposed model. The models described in the literature also showed more localized pressures on the heads of the metatarsals, while in the present model pressure was distributed more evenly.

The flatness of the foot surface studied herein (as captured by computed tomography) resulted in this more uniform distribution, unlike in models described in the previous literature, which had peak pressure points at the “center” of the heel. Regarding the presence of pressure points in the distal phalanges, the proposed model resembles that of Antunes et al. (2007)<sup>(7)</sup>, rather than Cheung and Zhang (2006)<sup>(8)</sup>. This may be due to center of pressure (COP) considerations.

The results obtained were compared with those of baropodometry. In the proposed model, the Achilles tendon force was not calculated; instead, we used the parameter reported by Hamill et al. (2016)<sup>(11)</sup>. The position of the center of pressure was obtained as shown in Figures 3C and 3D. Confrontation of the calculated COP against baropodometry shows that the Achilles tendon force does not correspond to 50% of the weight-bearing force in each foot. This is due to the fact that the COP was located elsewhere. Indeed, the physical therapist who performed baropodometry noted that the volunteer had genu recurvatum. The examination showed that peak pressure was exerted on the heel (~ 14.73N/cm<sup>2</sup>). There were no localized pressures on the heads of the metatarsals, only a large area of distributed pressure corresponding to the forefoot, with a peak pressure of 2.72N/cm<sup>2</sup>.

Finally, the difference in Achilles tendon forces may be due to the fact that Cheung and Zhang (2006)<sup>(8)</sup> modeled more than 100 ligaments to connect the bones (thus allowing the possibility of slight slippage between the bones) instead of geometrically generating cartilages to connect the bones (tie constraint), as was done in the present model.

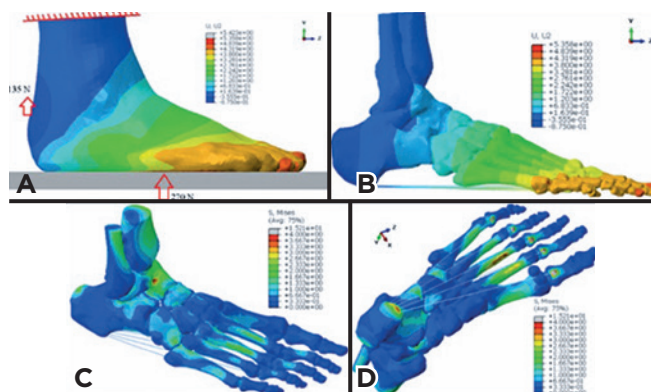


**Figure 2.** Distribution of displacements identified in the simulation: A, soft tissue; B, bone tissue; C and D, internal Von Mises stress distribution (MPa).

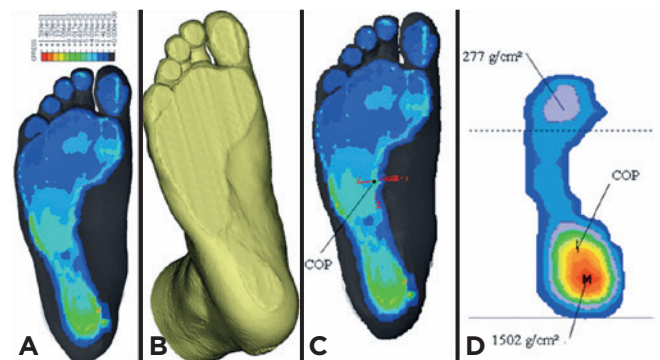


**Figure 3.** A and B, simulated model versus flat map of plantar surface; C and D, comparison between simulated model and baropodometry findings.

The clinical use of pressure distribution analysis through a finite element computational model, especially in patients with diabetic foot, should allow development of customized insoles by homogeneous weighting of foot pressure distribution, thus eliminating points of excessive stress at the foot-footwear-ground interface and helping prevent ulcers, infections, and amputations. The same technology can be offered to patients who have undergone partial amputations of the foot, redistributing stump pressures and avoiding further amputations.

## Conclusion

Finite element analysis provides a feasible, reproducible manner of reproducing the biomechanical behavior of healthy feet.

## Acknowledgements

The authors thank CNPq (grant no. 442138/2016-4 TA) and Universidade de Caxias do Sul (UCS) for funding; Materialise NV and Altair Brasil; and the staff at the UCS Clinical Center for their support.

**Authors' contributions:** Each author contributed individually and significantly to the development of this article: CAC \*(<https://orcid.org/0000-0001-5623-8411>) conceived and planned the activities that led to the study, wrote the article, participated in the review process, approved the final version; VVL \*(<https://orcid.org/0000-0002-5883-9613>) conceived and planned the activities that led to the study, data collection, research development; ALGS \*(<https://orcid.org/0000-0002-6672-1869>) research development, participated in the review process; VGA \*(<https://orcid.org/0000-0001-5836-8658>) data collection, interpreted the results of the study, research development, participated in the review process; PRL \*(<https://orcid.org/0000-0001-5334-290X>) data collection review, research development; FAC \*(<https://orcid.org/0000-0003-0507-6701>) wrote the article, participated in the review process. \*ORCID (Open Researcher and Contributor ID) .

## References

1. Porciúncula MVP, Rolim LCP, Garofolo L, Ferreira SBG. Analysis of factors associated with extremity ulceration in diabetic subjects with peripheral neuropathy. *Arq Bras Endocrinol Metab.* 2007; 51(7):1134-42.
2. Van Schie CH. A review of the biomechanics of the diabetic foot. *Int J Low Extrem Wounds.* 2005;4(3):160-70.
3. Codogno JS, Fernandes RA, Monteiro HL. Physical activity and healthcare cost of type 2 diabetic patients seen at basic units of healthcare. *Arq Bras Endocrinol Metab.* 2012;56(1):6-11.
4. Barceló A, Aedo C, Rajpathak S, Robles S. The cost of diabetes in Latin America and the Caribbean. *Bull World Health Organ.* 2003; 81(1):19-27.
5. Brasil. Ministério da Saúde. Secretaria de Atenção à Saúde. Departamento de Atenção Básica. Manual do pé diabético: estratégias para o cuidado da pessoa com doença crônica. Brasília, DF; 2016.
6. Cheung JT, Zhang M, Leung AK, Fan YB. Three-dimensional finite element analysis of the foot during standing--a material sensitivity study. *J Biomech.* 2005;38(5):1045-54.
7. Antunes PJ, Dias GR, Coelho AT, Rebelo F, Pereira T. Non-linear finite element modelling of anatomically detailed 3d foot model. 2007. Available from: [https://www.researchgate.net/publication/228399624\\_Non-Linear\\_Finite\\_Element\\_Modelling\\_of\\_Anatomically\\_Detailed\\_3D\\_Foot\\_Model](https://www.researchgate.net/publication/228399624_Non-Linear_Finite_Element_Modelling_of_Anatomically_Detailed_3D_Foot_Model).
8. Cheung JTM, Zhang M. Finite element modeling of the human foot and footwear. In: ABAQUS Users' Conference; 2006. p. 145-58.
9. Costa CA, Grandi S, Bona AF, Basso JRF. Manufacturing of custom seating devices for wheelchair users. *J Mech Engin Biomech.* 2019; 3(5):35-41.
10. Gefen A. Stress analysis of the standing foot following surgical plantar fascia release. *J Biomech.* 2002;35(5):629-37.
11. Hamill J, Knutzen KM, Derrick TR. Bases biomecânicas do movimento humano. 4a ed. São Paulo: Manole; 2016.